International Journal of Nanoelectronics and Materials
IJNeaM
ISSN 1985-5761 | E-ISSN 2232-1535

Effect of rotational speed on physical properties of Cu doped SnO_2 thin films

T. Bhima Raju [a,b] *, Y. Ramakrishna [a], and B. Rajesh Kumar [c]

[a]*Department of Engineering Physics, AUCE (A), Andhra University, Visakhapatnam-530045, A.P, India*
[b]*Department of Physics, ANITS (A), Sangivalasa-531162, Visakhapatnam, A.P, India*
[c]*Department of Physics, School of Sciences, GITAM (Deemed to be University), Visakhapatnam-530045, A.P, India*
**Corresponding author. Tel.: +91 8985886883, e-mail: physics24416@gmail.com*

Received 14 April 2025, Revised 14 November 2025, Accepted 20 January 2026

ABSTRACT

The sol-gel spin-coating (SGSC) technique, with rotational speed varied from 2000 to 3500 rpm, was employed to prepare Cu-doped SnO_2 (CTO) films. XRD patterns of the CTO films show a polycrystalline tetragonal structure. The reduction in crystallite size from 36 to 21 nm with increasing rotational speed supports the increase in microstrain. The rise in rotational speed promotes the formation of smaller crystallites because of rapid film solidification, which in turn increases microstrain owing to enhanced lattice distortions and grain-boundary effects. The morphology of the CTO films shows homogeneous growth with a spherical shape, and agglomerated grains were observed at higher rotational speeds. Cu-doped SnO_2 prepared at 3500 rpm shows an optimum transmittance of 82% in the visible region. The optical band-gap energy of Cu-doped SnO_2 films increased from 3.20 to 3.65 eV because of the Burstein-Moss effect. This study provides a novel correlation between lattice distortion (via basal plane angle) and surface roughness evolution in Cu-doped SnO_2 thin films, offering deeper insights into the structural-morphological relationship influencing their physical properties.

Keywords: *Cu doped SnO_2 thin films, X-ray diffraction, Surface morphology, Atomic force microscopy, Optical properties*

1. INTRODUCTION

Tin oxide (SnO_2) is a well-known wide-band-gap (~3.6 eV) semiconductor with n-type conductivity, which originates from intrinsic donor-type defects such as oxygen vacancies and tin interstitials [1, 2]. Nanostructured SnO_2 is widely used in gas sensors [3–5], as an electron transport layer in heterojunction GaAs-based solar cells [6–10], in transparent electrodes [11], in photodetectors, and in microelectronic applications [12, 13]. The structural characteristics of SnO_2, including crystallinity and the existence of flaws such as oxygen vacancies, interstitials, and surface defects, affect its physical properties. The properties of SnO_2 are influenced by crystallite size, crystallinity, shape, size distribution, and the addition of dopant materials. The defect chemistry and microstructure of the parent system are altered when an appropriate dopant is introduced into the parent crystal lattice [14], which also changes the structural, optical, and electrical properties. A variety of dopant materials, including Cu [15], Mg [16], and Sb [17], have been employed by researchers to adjust the characteristics of SnO_2. Copper (Cu) is one such dopant; it is a ductile metal with exceptional thermal and electrical conductivity. Because of its high biocompatibility, it is widely used as an antibacterial agent. Cu occurs stably in the +2 oxidation state, which leads to catalytic activity. When Sn^{4+} ions are replaced by Cu^{2+} ions, the main effect is the densification of oxygen vacancies. Cu doping enhances the structural and morphological properties of the host lattice by effectively producing localized free electrons at the surface defects of the host material SnO_2 [18, 19]. There are different reports on the preparation of Cu-doped SnO_2 films, such as spray pyrolysis [20], sol-gel methods [21, 22], the chemical bath deposition method [23], and magnetron sputtering [24]. Among these deposition techniques, the sol-gel spin-coating (SGSC) method is attractive because of its capacity to deposit over large areas, its precise stoichiometry control, its uniform film growth, its cost-effectiveness, and its ability to deposit at low temperatures.

From the literature survey, there are very few reports on the effect of rotational speed on spin-coated CTO films. In the present work, a systematic investigation of the effect of rotational speed on the morphological, structural, and optical properties of CTO films is reported.

2. EXPERIMENTAL DETAILS

Copper-doped tin oxide (CTO) films were prepared using the sol-gel process with $SnCl_2.2H_2O$ as the precursor, 2-methoxyethanol as the solvent, $Cu(CO_2CH_3)_2{\cdot}2H_2O$ as the dopant, and monoethanolamine (MEA) as the stabilizer to prepare the solution. The solution was stirred for two hours at 80°C. The synthesized solution was aged for 48 hours before being spin-coated. A spin coater (SpinNXG-P1 Apex Instruments, India) was used for the preparation of thin films by varying the rotational speed from 2000 to 3500 rpm. The films were dried at 150°C for 15 minutes in an oven. To achieve the required film thickness, this procedure was repeated three to five times. A spectroscopic ellipsometer (Alpha-SE, J.A. Woollam, USA; angle of incidence: 70°; focused beam diameter <1 mm; CompleteEASE software for data analysis) was used to measure the film thickness, and the resulting thickness

ranged from 145 to 240 nm. The structure of the CTO films was determined using a Bruker D8 X-ray diffractometer with Cu Kα radiation of 1.54056 Å, an operating voltage of 40 kV, a current of 30 mA, and a scanning range of 2θ = 10 to 70°. The surface morphology of the CTO films was analyzed using scanning electron microscopy (SEM, Ultra-55, Karl Ziess) at 15 kV with a working distance of 16.8 mm and atomic force microscopy (AFM, Bruker Dimension Icon; vertical resolution = 0.3 nm; lateral resolution = 10 nm depending on the tip). The elemental composition of the CTO films was recorded using energy-dispersive X-ray spectroscopy (EDS, Quantax 200) at a working voltage of 20 kV. A UV-Vis-NIR spectrophotometer (Hitachi U-2900; optical system: double beam; spectral band pass: 1.5 nm) was employed to measure the optical transmission spectra of the CTO films over the wavelength range of 300–2500 nm. The electrical resistivity of the CTO films was measured by the four-point probe method using a Keithley 2450 source meter.

3. RESULTS AND DISCUSSION

3.1. XRD Analysis

Figure 1 illustrates the variation in CTO film thickness with rotational speed varied from 2000 to 3500 rpm. The film thickness decreased from 240 to 145 nm as the rotational speed increased from 2000 to 3500 rpm. At higher rotational speed, the centrifugal force acting on both the solution and the substrate removes excess solution and leaves a smaller amount of solution to produce thin films on the glass substrate. For the same reason, longer deposition times result in thinner films. For each spin speed and deposition time, the deposition was performed at least three times to demonstrate the reproducibility of films with the same thickness. Overall, the film thickness exhibited an inverse proportionality to both spinning speed and time.

Figure 2 depicts the XRD profiles of CTO films prepared at different rotational speeds. All the diffraction peaks were indexed to the rutile tetragonal SnO_2 structure according to the reported data in JCPDS file no. 41-1445. No additional peaks were observed in the spectrum. The dominant peaks of the spectra correspond to the (1 1 0), (1 0 1), and (2 1 1) planes, as shown in Figure 2. It is noticed that the XRD peak intensities decrease with increasing rotational speed. It is well known that peak intensity is proportional to film thickness [25]. The Debye-Scherrer equation [26] was used to estimate the crystallite size, which was found to decrease from 36 to 21 nm with increasing rotational speed [27–29]. The lattice constants a and c increased from 0.4735 to 0.4794 nm and from 0.3230 to 0.3360 nm, respectively, with rotational speed, as listed in Table 1. This might be connected to the replacement of Cu^{2+} ions by Sn^{4+} ions in the crystal structure of Cu-doped SnO_2, since their ionic radii are similar in size (Cu^{2+} = 0.074 nm, Sn^{4+} = 0.069 nm). Additionally, the lattice arrangement between various planes improved the lattice constants of the films when Cu^{2+} ions replaced Sn^{4+} sites in the SnO_2 lattice. These results are in good agreement with previously reported literature [30, 31].

The microstructural parameters δ, σ, and Ed were estimated from the relations $\delta = 1/D2$, $\sigma = E \times \varepsilon$ (E ~ 200 GPa), and $Ed = 0.5 \times \varepsilon 2$ [32]. When the rotational speed increased from 2000 to 3500 rpm, the dislocation density of the CTO films increased from 7.70×10^{14} to 2.26×10^{15} /nm^2. Grain boundaries may arise more frequently as a result of crystallite-size reduction caused by increased rotational speed. The microstructural parameters of the CTO films are listed in Table 2.

From the SnO_2 unit cell, the apical (d_1) and equatorial (d_2) Sn-O distances are determined from Equations (1) and (2).

$$d_1 = \sqrt{2}ua \quad (1)$$

$$d_2 = \sqrt{2\left(\frac{1}{2}-u\right)^2 .a^2 + \left(\frac{c}{2}\right)^2} \quad (2)$$

The parameter u determines the position of O^{2-} ions at ±(u, u, 0) and ±(0.5+u, 0.5–u, 0.5), whereas a and c are lattice parameters and c/a = 2u. Each Sn^{4+} cation bonds

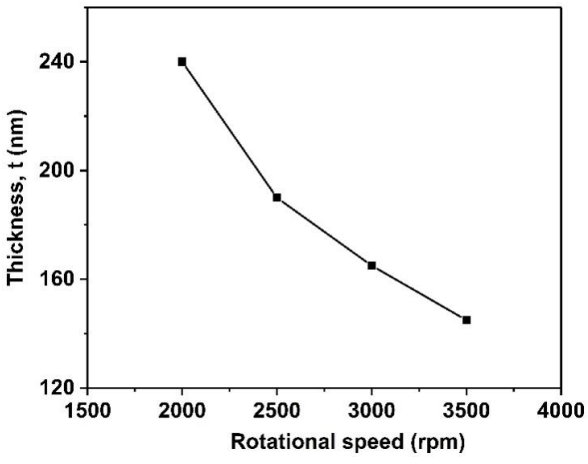

Figure 1. Plot of film thickness of CTO films with rotational speed

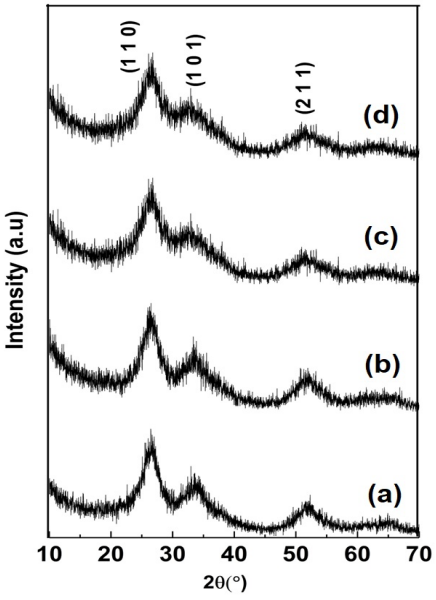

Figure 2. XRD patterns of CTO films deposited with (a) 2000, (b) 2500, (c) 3000, and (d) 3500 rpm

Table 1. Lattice constants, volume, and crystallite size of CTO films

Rotational speed (rpm)	Lattice constants		Volume, $V = a^2c$ $(Å)^3$	Crystallite size, D (nm)
	a (Å)	c (Å)		
2000	0.4735	0.3230	72.44	36
2500	0.4766	0.3289	74.67	27
3000	0.4783	0.3340	76.43	24
3500	0.4794	0.3360	77.23	21

Table 2. Microstructural parameters of CTO films

Rotational speed (rpm)	$\varepsilon \times 10^{-3}$ $(line^{-2}.m^{-4})$	$\delta \times 10^{15}$ (nm^{-2})	σ (GPa)	$E_d \times 10^6$ $(J.m^{-3})$
2000	12.05	2.07	2.41	14.52
2500	13.33	1.19	2.66	17.77
3000	13.84	0.73	2.77	19.16
3500	14.18	0.34	2.83	20.11

Table 3. d_1, d_2, and θ values of CTO films

Rotational speed (rpm)	u	c/a	d_1 (Å)	d_2(Å)	θ (°)
2000	0.3410	0.6820	2.284	1.934	25.06
2500	0.3451	0.6902	2.325	1.947	24.82
3000	0.3491	0.6982	2.362	1.957	24.18
3500	0.3504	0.7008	2.375	1.962	23.97

with each O^{2-} anion in a precise tetragonal configuration, resulting in perfect octahedral coordination [33]. The basal plane angle (θ) is determined from the equation: $\cos\theta = [a^2(1-4u+8u^2)-1]/[c^2+4a^2(0.5-u)^2+4a^2u^2]$ [34]. When Cu^{2+} ions replace Sn^{4+} ions, the octahedral symmetry becomes less distorted, leading to a decreasing tendency of d_1 and d_2 with an increase in the basal angle (θ). Table 3 lists the d_1, d_2, and θ values obtained for the CTO films.

3.2. Surface Morphological Analysis

SEM micrographs of CTO films deposited by varying rotational speeds from 2000 to 3500 rpm are shown in Figure 3. All samples have a compact, dense, and homogeneous surface with a large number of grouped grains. The films made at 3000 and 3500 rpm had smooth surfaces with tiny spherical grains. The EDS pattern of the CTO thin film prepared at 3000 rpm is depicted in Figure 4. The EDS spectra revealed the presence of tin (Sn), oxygen (O), and copper (Cu) in the CTO film. The Cu-related peak in the EDS spectrum confirms the presence of Cu dopant in the SnO_2 lattice. The corresponding quantitative atomic percentages of Sn, Cu, and O are 63.08%, 31.67%, and 5.25%, respectively. The O Kα line has a very low energy (~0.52 keV). At such low energies, X-rays are easily absorbed by the detector window, the sample, or even the air path between the sample and the detector. This absorption distorts and broadens the oxygen peak.

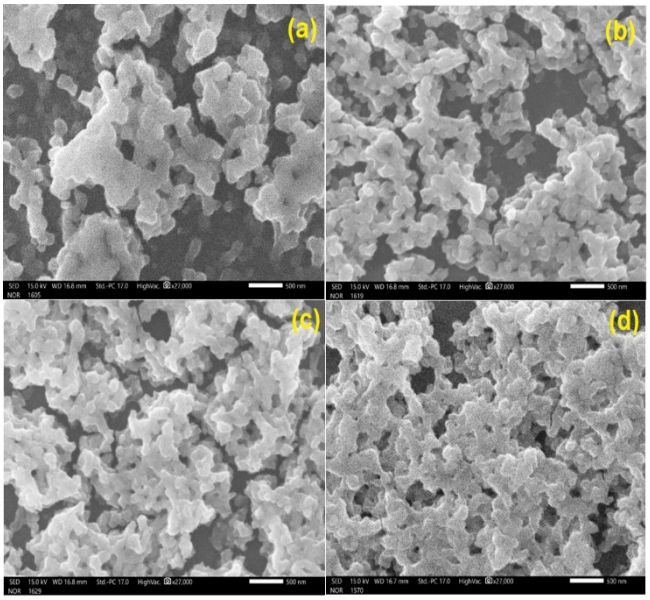

Figure 3. SEM images of CTO films (a) 2000, (b) 2500, (c) 3000, and (d) 3500 rpm

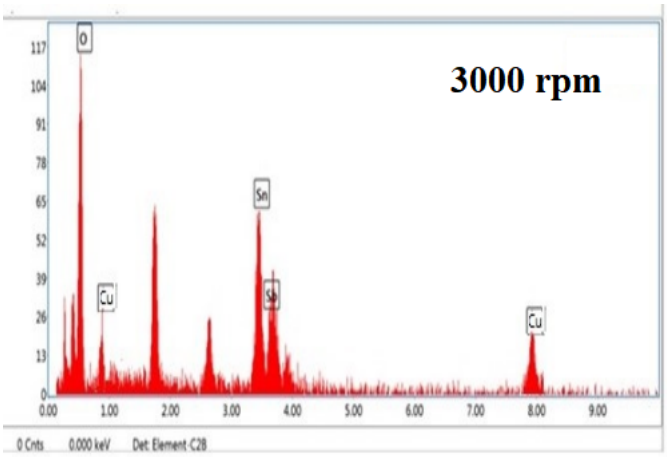

Figure 4. EDS of the CTO film

AFM micrographs (2 × 2 μm²) of the CTO films are shown in Figure 5. The morphology shows grain aggregation and a surface free of cracks. The presence of well-segregated grains is indicated by the numerous hills and valleys formed throughout the studied region at higher rotational speeds. Table 4 lists the roughness parameters of average roughness (R_a), roughness kurtosis (R_{ku}), roughness skewness (R_{sk}), and root-mean-squared roughness (R_q or R_{rms}) for the CTO films. The CTO films exhibit positive surface skewness, representing the existence of many bumps. As crystallization diminishes, the films prepared at higher rotational speeds exhibit a considerably rougher surface with no grain enhancement. Grain-size reduction,

Table 4. Roughness parameters of CTO films

Rotational speed (rpm)	R_q (nm)	R_a (nm)	R_{ku}	R_{sk}
2000	5.85	4.55	0.237	3.415
2500	6.15	5.68	0.054	3.083
3000	7.26	6.51	0.735	4.242
3500	8.17	7.37	0.715	4.854

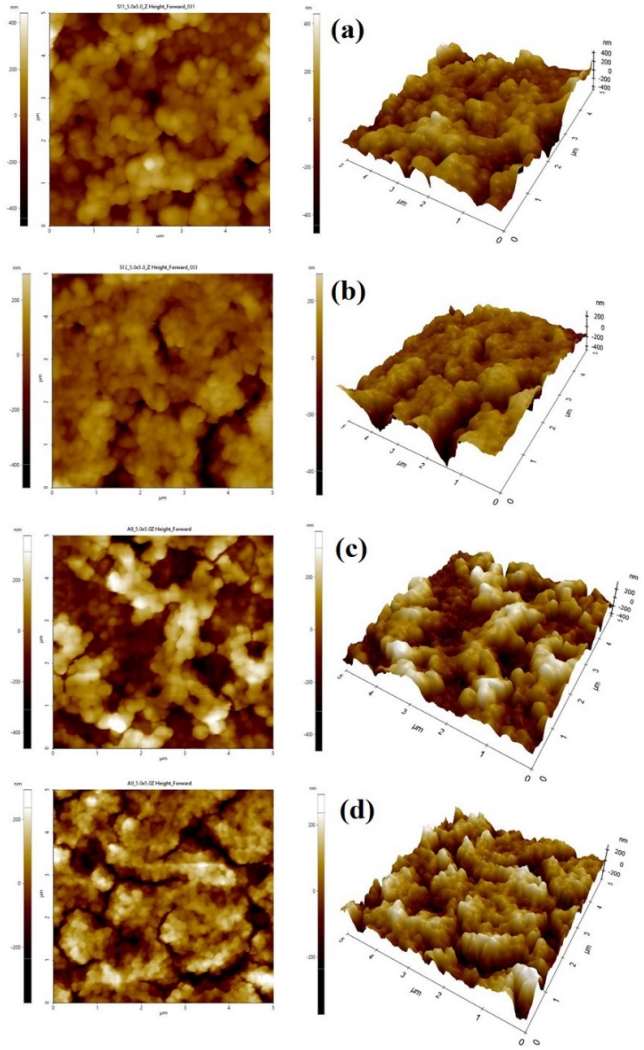

Figure 5. AFM images of CTO films (a) 2000, (b) 2500, (c) 3000, (d) 3500 rpm

surface defects, and strain that develops during growth are the reasons for the increased surface roughness as spin speed increases. The observed reduction in grain size suggests a deterioration in crystalline quality, which is confirmed by the XRD results.

3.3. Optical Analysis

Optical transmittance spectra of CTO films prepared at various rotational speeds are illustrated in Figure 6(a). As the rotational speed increases, the transmittance increases, whereas the film thickness decreases from 220 to 160 nm because of the reduced film density. The transparency of the films increases as the film thickness decreases because fewer photons are absorbed. CTO films were found to be transparent at higher wavelengths and opaque at lower wavelengths. The decrease in light scattering due to reduced film thickness explains the increase in optical transmittance. The optical band gap of the CTO films was determined from Tauc's equation [35].

$$(\alpha h\nu) = A\,(h\nu - E_g)^n \quad (3)$$

Here, m indicates the optical transition process, A is a constant that depends on the nature of the transition, and α is the absorption coefficient. The optical band-gap energy (Eg) of the CTO films, estimated from the Tauc plot of $(\alpha h\nu)^2$ versus hν, is depicted in Figure 6(b). Eg shifted from 3.20 to 3.65 eV with increasing rotational speed because of the Burstein-Moss (B-M) effect [36]. As the band gap widens due to the B-M effect, the carrier concentration increases. The carrier concentration of the CTO films increased from 3.85×10^{21} to 4.69×10^{21} cm^{-3} with increasing rotational speed. These findings are consistent with previously reported literature [37–40].

The edge potentials for VB and CB (E_{VB} and E_{CB}) were estimated from [41]:

$$E_{VB} = \chi - E_e + 0.5E_g \quad (4)$$

$$E_{CB} = E_{VB} - E_g \quad (5)$$

Here, Ee (~4.5 eV) is the free-electron energy, and χ (~6.24 eV) is the electronegativity. Therefore, the EVB values for CTO films prepared at 2000, 2500, 3000, and 3500 rpm were obtained as 3.56, 3.50, 3.40, and 3.34 eV, whereas the corresponding ECB values were –0.085, –0.02, 0.08, and 0.14 eV.

The decrease in refractive index at shorter wavelengths shown in Figure 7(a) is due to the increase in absorption caused by the enhanced packing density of the films [42, 43]. The extinction coefficient values increased with wavelength, as shown in Figure 7(b), because of the higher number of defect states [44].

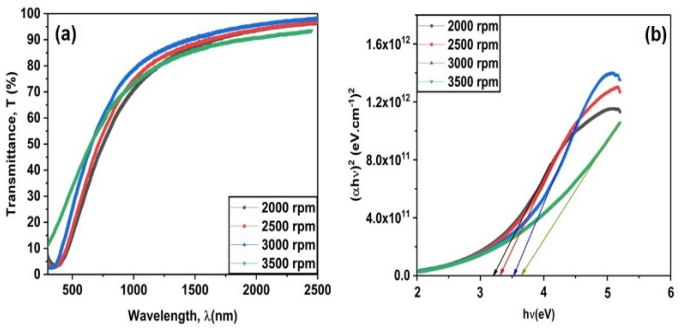

Figure 6. (a) Optical transmittance spectra (b) Tauc's plot of CTO films

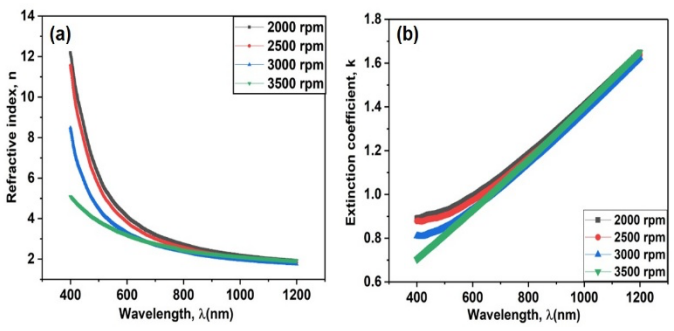

Figure 7. Plot of (a) refractive index and (b) extinction coefficient with wavelength for CTO films

3.4. Electrical Properties

The electrical resistivity of the CTO films measured by the four-point probe method was obtained as 2.12×10^{-3}, 1.52×10^{-3}, 1.16×10^{-3}, and 0.86×10^{-3} Ω.cm for 2000, 2500, 3000, and 3500 rpm, respectively. The sheet-resistance values for the CTO films were calculated using the formula $R_s = \rho/t$. The R_s values for CTO films prepared at 2000, 2500, 3000, and 3500 rpm were obtained as 88.3, 72.4, 61.1, and 59.3 Ω/sq, respectively. The decrease in sheet resistance with increased rotational speed is due to improved free-carrier concentration.

4. CONCLUSION

Cu-doped SnO_2 thin films were deposited by the SGSC technique at rotational speeds from 2000 to 3500 rpm. XRD patterns of the CTO films exhibit a tetragonal rutile phase with a preferred orientation along (1 0 1). The crystallite size decreased from 36 to 21 nm with increasing rotational speed. The surface morphology of the CTO films exhibits dense grains in agglomerated form. The transmittance spectra of the CTO films increased with increasing rotational speed because of the reduced film thickness. The optical band gap of the CTO films widened from 3.20 to 3.65 eV with rotational speed because of the B-M effect. These results reveal that the prepared CTO films have an interesting capability to tune physical properties through rotational speed, which makes them promising for various optoelectronic applications.

REFERENCES

[1] M. Kumar, A. Kumar, and A. C. Abhyankar, "Influence of texture coefficient on surface morphology and sensing properties of W-doped nanocrystalline tin oxide thin films," *ACS Applied Materials & Interfaces,* vol. 7, no. 6, pp. 3571–3580, 2015.

[2] M. Li, C. Mou, Y. Zhang, X. Li, H. Zhu, and G. Wei, "Zn-doped SnO_2 nanoparticles for ethanol vapor sensor: a combined experimental and first-principles study" *Journal of Materials Science: Materials in Electronics,* vol. 34, pp. 1059/1–15, 2023.

[3] L. Wang, J. Li, Y. Wang, K. Yu, X. Tang, Y. Zhang, S. Wang, and C. Wei, "Construction of 1D SnO_2-coated ZnO nanowire heterojunction for their improved n-butylamine sensing performances,"*Scientific Reports,* vol. 6, no. 1, pp. 1–12, 2016.

[4] U. Garduño Terán, A. I. Díaz Cano, T. Torchynska, I. C. Ballardo Rodriguez, B. El Filali, and J. E. Cervantes," Impact of Cu doping on morphology, structural and optical characteristics of SnO_2 thin films prepared by spray pyrolysis," MRS Advances, vol. 9, no. 6, pp. 1849–1853, 2024.

[5] W. Liu, Q. Kang, L. Wang, L. Wen, and Z. Li, "Improved performance of Zn-doped SnO_2 modified g-C_3N_4 for visible light-driven photocatalysis," *Environmental Science and Pollution Research,* vol. 29, pp. 51989–52002, 2022.

[6] H. J. Snaith and C. Ducati, "SnO_2-Based Dye-Sensitized Hybrid Solar Cells Exhibiting Near Unity Absorbed Photon-to-Electron Conversion Efficiency," *Nano Letters,* vol. 10, no. 4, pp. 1259–1265, 2010.

[7] A. S. Al-Ezzi and M. N. M. Ansari, "Numerical analysis and performance study of a double-heterojunction GaAs-based solar cell," *Journal of Computational Electronics*, vol. 23, pp. 358–368, 2024.

[8] A. S. Al-Ezzi, M. N. M. Ansari, S. K. Ahmed, N. M. L. Tan, N. A. Nordin, and S. M. Nomanbhay, "Analytical modelling, simulation and comparative study of multi-junction ($GaInP_2$ /InGaAs/Ge) solar cell efficiency," *Journal of Computational Electronics*, vol. 22, pp. 1048–1060, 2023.

[9] A. S. I. Al-Ezzi and M. N. M. Ansari, "Analytical modelling and performance study of single-junction GaAs-based solar cell efficiency," *Journal of the Korean Physical Society*, vol. 86, pp. 245–262, 2025.

[10] A. S. Al-Ezzi, M. N. M. Ansari, and N. Tan, "Flexible and freestanding solar cells based on metal organic chemical vapour deposition grown graphene," *Chemical Papers*, vol. 79, pp. 2019–2036, 2025.

[11] C. Terrier, J. P. Chatelon, R. Berjoan, and J. A. Roger, "Sb-doped SnO_2 transparent conducting oxide from the sol-gel dip-coating technique," *Thin Solid Films*, vol. 263, no. 1, pp. 37–41, 1995.

[12] S. Huang, H. Wu, M. Zhou, C. Zhao, Z. Yu, Z. Ruan, and W. Pan, "A flexible and transparent ceramic nanobelt network for soft electronics," *NPG Asia Materials*, vol. 6, no. 2, p. e86, 2014.

[13] S. Brovelli, N. Chiodini, R. Lorenzi, A. Lauria, M. Romagnoli, and A. Paleari, "Fully inorganic oxide-in-oxide ultraviolet nanocrystal light emitting devices," *Nature Communications,* vol. 3, no. 1, p. 690, 2012.

[14] A. Kar, S. Kundu, and A. Patra, "Surface Defect-Related Luminescence Properties of SnO_2 Nanorods and Nanoparticles," *Journal of Physical Chemistry C*, vol. 115, no. 1, pp. 118–124, 2011.

[15] P. Chetri, B. Saikia, and A. Choudhury, "Structural and optical properties of Cu doped SnO_2 nanoparticles: An experimental and density functional study," *Journal of Applied Physics*, vol. 113, no. 23, p. 233514, 2013.

[16] N. Mazumder, A. Bharati, S. Saha, D. Sen, and K. K. Chattopadhyay, "Effect of Mg doping on the electrical properties of SnO_2 nanoparticles," *Current Applied Physics*, vol. 12, no. 3, pp. 975–982, 2012.

[17] Q. Wei, P. Song, Z. Li, Z. Yang, and Q. Wang, "Hierarchical peony-like Sb-doped SnO_2 nanostructures: Synthesis, characterization and HCHO sensing properties," *Materials Letters,* vol. 191, pp. 173–177, 2017.

[18] S. Nilavazhagan, S. Muthukumaran, and M. Ashokkumar, "Microstructural and band gap exploration on Ni-doped SnO_2 nanoparticles co-doped with Cu," *Journal of Materials Science: Materials in Electronics*, vol. 26, no. 6, pp. 3989–3996, 2015.

[19] M. Parthibavarman, V. Hariharan, C. Sekar, and V. N. Singh, "Effect of copper on structural, optical and electrochemical properties of SnO_2 nanoparticles," *Journal of optoelectronics and advanced materials*, vol. 12, p. 1894, 2010.

[20] P. S. Kolhe, S. G. Kulkarni, N. Maiti, and K. M. Sonawane, "Effect of Cu doping concentration on H_2S gas-sensing properties of Cu-doped SnO_2 thin films," *Applied Physics A*, vol. 125, no. 372, 2019.

[21] N. L. Myadam, D. Y. Nadargi, J. D. Nadargi, and M. G. Chaskar, "Cu/SnO_2 xerogels: a novel epoxide derived nanomaterial as formaldehyde gas sensor," *Journal of Sol-Gel Science and Technology*, vol. 96, no. 1, pp. 56–66, 2020.

[22] V. S. Jahnavi, S. K. Tripathy, and A. V. N. R. Rao, "Study of the structural, optical, dielectric, and magnetic properties of copper-doped SnO_2 particles," *Journal of Electronic Materials*, vol. 49, pp. 3540–3554, 2020.

[23] S. I. Abbas, S. F. Hathot, A. S. Abbas, and A. A. Salim, "Influence of Cu doping on structure, morphology, and optical characteristics of SnO_2 thin films prepared by chemical bath deposition technique," *Optical Materials*, vol. 117, p. 111212, 2021.

[24] N. Somjaijareon, R. Sakdanuphab, N. Chanlek, P. Chirawatku, and A. Sakulkalavek, "Simultaneous O_2 plasma and thermal treatment for improved surface conductivity of Cu-Doped SnO_2 films," *Vacuum*, vol. 166, pp. 212–217, 2019.

[25] T. V. K. Karthik, A. G. Hernandez, M. L. de la Olvera, A. Maldonado, and H. Gómez Pozos, "Effect of Au and Ag contacts on the CO sensitivity of SnO_2 thick films, "*Journal of Materials Science: Materials in Electronics*, vol. 31, pp. 7481–7489, 2020.

[26] C. Yang, M. Chen, J. Wang, and H. Lu, "Zn-Doped SnO_2 Compact Layer for Enhancing Performance of Perovskite Solar Cells," *International Journal of Photoenergy*, vol. 2021, pp. 1–10, 2021

[27] P. Gupta and S. K. Sharma, "A study of oxygen gas sensing in Zn-doped SnO_2 nanostructures," *Materials Research Express*, vol. 4, no. 6, p. 065010, 2017.

[28] Q. Zhao, D. Ju, X. Deng, J. Huang, B. Cao, and X. Xu, "Morphology-modulation of SnO_2 Hierarchical Architectures by Zn Doping for Glycol Gas Sensing and Photocatalytic Applications," *Scientific* Reports, vol. 5, no. 1, p. 7874, 2015.

[29] S. Kumaravelan, S. Seshadri, R. Suresh, K. Ravichandran, P. Sathishkumar, K. Shanthaseelan, and N. Suganthi, "Effect of Zn dopant on SnO_2 nano-pyramids for photocatalytic degradation," *Chemical Physics Letters*, vol. 769, p. 138352, 2021.

[30] Zulfiqar, Y. Yuan, Q. Jiang, J. Yang, L. Feng, W. Wang, Z. Ye, and J. Lu, "Variation in luminescence and bandgap of Zn-doped SnO_2 nanoparticles with thermal decomposition," *Journal of Materials Science: Materials in Electronics*, vol. 27, no. 9, pp. 9541–9549, 2016.

[31] I. Karaduman Er, M. Ali Yıldırım, H. Hasan Örkçü, A. Ateş, and S. Acar, "Structural, morphological and gas sensing properties of $Zn_{1-x}Sn_xO$ thin films by SILAR method," *Applied Physics A*, vol. 127, no. 4, pp. 1–14, 2021.

[32] A. A. Ahmad, A. B. Migdadi, and Q. M. Al-Bataineh, "Structural, optical, and electrical properties of strontium-doped tin dioxide films for high photoconductivity," *Thin Solid Films*, vol. 796, p. 140312, 2024.

[33] S. Das and V. Jayaraman, "SnO_2: A comprehensive review on structures and gas sensors," *Progress in Materials Science*, vol. 66, pp. 112–255, 2014.

[34] F. H. Aragon, J. A. H. Coaquira, L. Villegas-Lelovsky, S. W. da Silva, D. F. Cesar, L. C. C. M. Nagamine, R. Cohen, E. Men´ endez-Proupin, and P. C. Morais, "Evolution of the doping regimes in the Al-doped SnO_2 nanoparticles prepared by a polymer precursor method," *Journal of Physics: Condensed Matter*, vol. 27, no. 9, p. 095301, 2015.

[35] M. Ali Yıldırım and A. Ateş, "Influence of films thickness and structure on the photo-response of ZnO films," *Optics Communications*, vol. 283, pp. 1370–1377, 2010.

[36] J. Sawahata and T. Kawasaki, "Structural and electrical properties of Sb-doped SnO_2 thin films prepared by metal organic decomposition," *Thin Solid Films*, vol. 685, pp. 210–215, 2019.

[37] A. S. Ahmed, M. Shafeeq, M. L. Singla, S. Tabassum, A. H. Naqvi, and A. Azam, "Band gap narrowing and fluorescence properties of nickel doped SnO_2 nanoparticles," *Journal of Luminescence*, vol. 131, pp. 1–6, 2011.

[38] M. E. Guluduren, "Characterization of Zn-doped SnO_2 thin films prepared by the SILAR technique for optoelectronic applications," *Semiconductor Science and Technology*, vol. 36, p. 095034, 2021.

[39] A. G. Habte, F. G. Hone, and F. B. Dejene, "Zn doping effect on the properties of SnO_2 nanostructure by co-precipitation technique," *Applied Physics A*, vol. 125, no. 6, p. 402, 2019.

[40] D. Meena, V. K. Verma, Divya, Prerna, and S. Rana, "Investigation the effect of Zn doping on structural and optical properties of SnO_2," *Materials Today: Proceedings,* vol. 51, pp. 554–560, 2022.

[41] J. Wang, C. Lu, X. Liu, Y. Wang, Z. Zhu, and D. Meng, "Synthesis of tin oxide (SnO & SnO_2) micro/nanostructures with novel distribution characteristic and superior photocatalytic performance," *Materials and Design,* vol. 115, pp. 103–111, 2017.

[42] H. P. Dang, Q. H. Luc, V. H. Le, and T. Le, "The influence of deposition temperature and annealing temperature on Ga-doped SnO_2 films prepared by direct current magnetron sputtering," *Journal of Alloys and Compounds*, vol. 687, pp. 1012–1020, 2016.

[43] T. Le, H. P. Dang, Q. H. Luc, and V. H. Le, "A study of structural, electrical, and optical properties of p-type Zn-doped SnO_2 films versus deposition and annealing temperature," *Journal of Physics D: Applied Physics*, vol. 50, no. 14, p. 145102, 2017.

[44] S. I. Abbas, S. F. Hathot, A. S. Abbas, and A. A. Salim, "Influence of Cu doping on structure, morphology, and optical characteristics of SnO_2 thin films prepared by chemical bath deposition technique," *Optical Materials*, vol. 117, p. 111212, 2021.